Calibration, traceability and uncertainty issues in surface texture metrology Version 2

NMS Programme for Length 1997 - 1999
Milestone 2.6.6

Richard K Leach
Dimensional & Optical Metrology Team
Centre for Basic, Thermal and Length Metrology
National Physical Laboratory
Queens Road
Teddington
Middlesex
United Kingdom
TW11 0LW

Abstract

Achieving consistent surface texture measurements is of vital importance to the performance of many components in well-established fields such as mechanical engineering and manufacturing, and is becoming increasingly important in the emerging field of nanotechnology. The route to traceability in surface texture measurements is still ill-defined and it is very uncommon to find a measured surface texture parameter presented with its associated uncertainty. This report summarises the methods used to calibrate surface texture measuring instruments and discusses the various ISO standards in the field. An uncertainty analysis of a fully traceable two-dimensional surface texture measuring instrument: NanoSurf IV, is undertaken and the uncertainties in measured surface texture parameters are analysed.

ISSN 1361-4088

National Physical Laboratory
Queens Road, Teddington, Middlesex, United Kingdom, TW11 0LW

Approved on behalf of the Managing Director
by Dr David Robinson, Head of Centre for Basic, Thermal and Length Metrology

CONTENTS

FIGURE LEGENDS

TABLES

NOMENCLATURE

Note: Surface texture parameters, for example *Ra*, are defined in table 5.14.

Section 1

$g(s)$	general function of fringe dispersion
δ	a small error in $g(s)$
h	a step height measurement
s	fringe dispersion
σ_s	variance in the measurement of s
n	integer fringe number
λ	the wavelength of light

Section 5

$u_c(x)$	combined standard uncertainty in a measurement of x
$u(x)$	standard uncertainty in a measurement of x
L	length measurement made using an interferometer
c_i, c_{ij}, c_{ijj}	partial derivatives of the model equation
i, j	subscripts
ν	degrees of freedom
n	number of measurements
u_{eff}	effective number of degrees of freedom
U	expanded uncertainty
k	coverage factor
L_ϕ	displacement measured by a two-beam interferometer
λ	wavelength of light
$\Delta\phi$	difference in phase from the reference and measurement arms
L_Ω	correction for diffraction
L_n	correction due to the change in air refractive index
L_t	correction for thermal effects on the metrology frame
L_m	correction for mechanical effects on the metrology frame
L_A	correction for imperfect optics and stray beams
L_d	correction for the dead path length
L_T	correction for air turbulence
L_j	correction for the measurement set-up

λ_0	fringe displacement
k	wavenumber
w_0	waist of a laser beam
u	aperture radius
w_f	defined by equation (5.13)
b	defined by equation (5.14)
D	absolute distance of the lens from the waist of the beam
f	focal length
s''	image to lens distance
s	object to lens distance
z_R	Rayleigh length
m	magnification
α	misalignment angle
z	distance between waist and detector
l	distance between waist and retro-reflector
θ	defined in the text
v	defined in the text
σ	defined in the text
λ_{vac}	wavelength of light in a vacuum
n	refractive index of air
σ	wavenumber
x	carbon dioxide content
t	air temperature
p	air pressure
f	water vapour partial pressure
t_{dp}	dewpoint temperature
$a(x, y)$	complex amplitude at point (x, y)
$\phi(x, y)$	phase of light at point (x, y)
$a_s(x, y)$	complex amplitude of stray light at point (x, y)
$\phi_s(x, y)$	phase of stray light at point (x, y)
p	path difference between stray light and test beams
I	intensity

D	dead path length
N	half the number of fringes counted during a displacement
n_2	refractive index at the end of a measurement
Δn	change in refractive index
d	displacement
z	vertical axis
x	axis of scan
a	intercept on z axis
b	gradient
χ	least-squares minimisation parameter
a^*	least-squares intercept on z axis
b^*	least-squares gradient
$S, S_x, S_z, S_{xx}, S_{zz}, S_{zx}$	summations defined by equations (5.46)
d	constant of proportionality
r	population correlation coefficient
f	defined in equation (5.55)
N	number of data points
μ_2	second moment

1. INTRODUCTION

Only in recent years have sound metrological principles been applied to the measurement of surface texture. Demonstration of true traceability of surface texture measurements is still rare and often only achieved by the time-consuming task of measuring the characteristics of the separate elements that make up the instrument. There are many different artefacts that can be used to characterise an instrument and a huge number of parameters that can be calculated from the measured data. There is a vast library of specification standards on the subject. The report will only consider those published by the International Standards Organisation (ISO). It is also rare to see an uncertainty figure quoted with a measured surface texture parameter - a taboo in dimensional metrology not seeming to cover surface texture. The aims of this report are to summarise the work to date on calibration of surface texture instruments and their associated uncertainties, to outline and discuss the relevant ISO standards and to carry out an uncertainty analysis for a fully traceable instrument developed at NPL. The results of this uncertainty analysis will then be extended to cover the surface texture parameters that would be calculated from the measured height and length data from the instrument. No attempt has been made in this analysis to examine the effects of the surface-probe interaction or the dynamic effects of scanning - it is assumed that the probe has perfect fidelity with the surface. For this reason NanoSurf IV is always operated as close to these conditions as possible, dynamic and static filtering due to the measurement process are assumed to limit the bandwidth of the instrument, not its measurement uncertainty.

2. CALIBRATION OF SURFACE TEXTURE MEASURING INSTRUMENTS (A HISTORY)

The metrological issues described in this section have been explored since the 1930s when the first surface texture instruments were being used. The traditional method of calibrating a surface texture measuring instrument is to traverse a lined calibration artefact. The period and amplitude of the lines would be chosen to, ideally, encompass the whole operating bandwidth of the instrument or its transmission characteristics. One of the early standards took the form of acid-etched lines in a substrate and was developed by Timms of NPL (1946). Underwood (also of NPL) introduced his Caliblocks in 1953 which were formed with a diamond tool mounted in a dividing engine and used to rule electro-deposited gold. Schobinger (1956) made specimens by vacuum coating glass surfaces with silica through a wire mask. These early artefacts had limited topography and could not match the lower spatial bandwidth limits of the instruments they were designed to calibrate.

Sharman of the National Engineering Laboratory (NEL) (1967) was, perhaps, the first to introduce essentially sinusoidal gratings as artefacts. These were formed by vacuum depositing aluminium and chromium on a lapped steel substrate and for a given peak-to-peak height a single specimen could be used to generate any pitch from 0.25 μm to 13 μm. The pitch variation was achieved by mounting the specimen on a small rotary table and rotating the specimen relative to the direction of traverse of the pick-up head. Much of the literature suggests the use of step-height standards, such as wrung gauge blocks for low magnification and lever arm devices or evaporated or etched films for high magnifications (Reason 1967).

Van Hasselt & Bruin (1963) and Bendeli, Duruz, *et. al.* (1974) introduced the idea of using a vibrating platform to simulate the spatial frequencies present in a surface. Calibration of a stylus instrument requires low frequency or static calibration to determine scale and linearity of the low frequency recording equipment. Also, dynamic calibration is necessary for transmission characteristics of averaging instruments with meter readouts. They suggest that the problems with using standard artefacts are the difficulty in obtaining satisfactory accuracies for static calibrations at very high magnifications (50 000x and above) without having to rely on the trueness of the attenuators and the effect of the finite shape of the stylus. Their method is, of course, limited to stylus instruments.

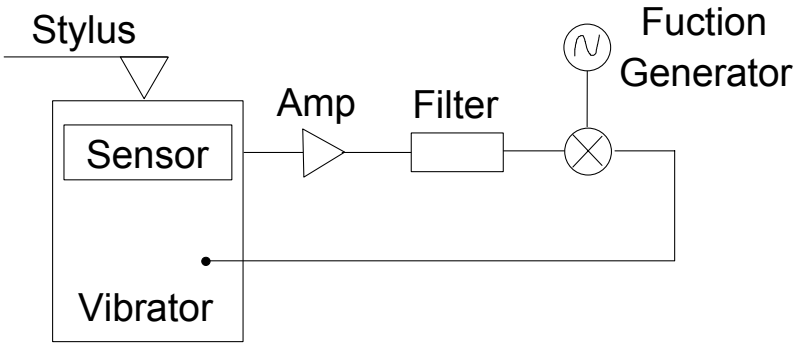

Figure 2.1 Vibrating stylus calibration rig, from Bendeli, Duruz, *et. al.* (1974)

Bendeli's instrumentation is shown in figure 2.1 and its operation is fairly self evident. The method has the following features:

- it provides a measurement of scale factor and linearity of low frequency recorders;
- it provides a measurement of transmission characteristics by applying a random signal to the vibration platform;
- it calibrates parameter meters by applying signals that generate desired profile shapes and characteristics;
- its displacement range is equal to ± 2 μm with -3 dB cut-off point at 800 Hz;
- calibration is via a spherical-ended capacitance probe with an AC resistance bridge, resolution 2 nm;
- its sensitivity is equal to 0.543 V μm^{-1} ± 0.5% per month;
- its non-linearity is less than 25 nm at extremities, but 10 nm over ± 1.5 μm.

Teague (1978) used interferometrically determined step-heights to calibrate other surface texture measuring instruments. The main sources of error using this technique are due to the geometry of the step (microscopic surface texture of the sides, non-flat surfaces and non-parallel planes) and errors in the interferometry. Teague derived a formula for the normalised uncertainty in a step height measurement, *h*, which is simply re-stated here

$$\frac{\delta h}{h} = \frac{\sigma_s}{h(n,s)}\left[1+\left(\frac{\mathrm{d}\delta}{\mathrm{d}s}\right)^2\right]^{\frac{1}{2}} \tag{2.1}$$

where *h* is given by

$$h = (n + g(s))\frac{\lambda}{2} \tag{2.2}$$

and n is the integer fringe number, $g(s)$ is a general function of the fringe dispersion, s (the lateral fringe displacement over the fringe spacing), λ is the wavelength of light, σ_s is the variance in the measurement of s and δ is a small error in $g(s)$. Teague then used least-squares methods to calculate the step-height from the measurement data and proved that the uncertainty in assigning a height value to a stylus step-profile is approximately equal to the *Ra* or *Rq* of the step's surface texture.

Tsukada & Kanada (1986) describe how it is difficult to specify, for an entire surface, any averaging parameter due to the enormous amount of data required. They also discussed the difficulties with relating the surface texture tolerances stated on real engineering drawings to the statistical surface texture parameters. By carrying out repeated measurements at different points on the same surface they reached the following conclusions:

- two-dimensional parameters, such as *Ra*, *Rq* and *Rz* when measured locally at different points on a surface, fluctuate according to a Gaussian distribution;
- each sample standard deviation, *S*, has a strong correlation with the population mean *F* and it can be expressed by $S = hF$ (h being a constant);
- three-dimensional surface texture parameters are larger than their two-dimensional brethren.

Whitehouse (1988) discussed the various sources of uncertainty when measuring surface texture with a stylus instrument. He suggested using ruled or etched standards or crystal lattice spacings as calibration artefacts and discussed the need for a knowledge of the inherent elasticity in the instrument being used. He also advocated using x-ray interferometry to calibrate stylus instruments and described a system developed at Warwick University (Chetwynd, Siddons, *et. al.* 1983). The most critical area, with x-ray techniques, was the mechanical interface between the silicon monolith and the transducer.

Song (1988) discussed the use of D-type random profile specimens for calibration of surface texture instruments (see §3 on standards for a fuller description of a D-type specimen). The disadvantages of the D-type specimens were:

- *Ra* range limited from 1.5 to 0.2 μm;

- no smooth datum plane at both sides of the measuring area - this makes comparisons awkward;
- large measurement error resulting from the phase error between the skid and stylus.

Song produced many more random profile specimens to overcome these problems.

Griffith & Grigg (1993) suggested using carbon-60 and other fullerene-like structures as calibration artefacts for surface texture measuring instruments requiring nanometre spacings. Franks (1993) used Amplitude-Wavelength space (Stedman 1987) to investigate the performance of various instruments and suggested ways of correlating different probing types by assessing the strength of their surface-probe interaction. Jörgensen, Garnoes, *et. al.* (1997) used waffle-plates to measure lateral non-linearity of scanning probe instruments and Fourier techniques to analyse the measurement data.

Haitjema (1997) reported on a EUROMET project (number 301) that compared methods of measuring depth-setting standards (step-heights). The project involved measuring five standards with groove widths of 0.01 mm and 0.1 mm and nominal depths of 32 nm, 64 nm, 160 nm, 1 μm and 3.2 μm. The samples were silicon substrates with a chromium overcoat and the definition of the groove was taken from ISO 5436. Instruments used were the Form Talysurf, Talystep, Nanostep and interference microscopes. If possible, participants were asked to carry out tests on the homogeneity of the specimens and the sensitivity of the depths to their definitions. Results showed that the depths are not sensitive to the definition to within a nanometre. The depth results were in good agreement for the small depths but the 3.2 μm standard gave a sample standard deviation of around 40 nm. Haitjema suggests that this situation must improve and that agreement should be within 1% (*i.e.* 30 nm in 3 μm).

NPL has been producing a number of sinusoidal specimens with varying period and amplitude to be used for calibrating surface texture measuring instruments (NMS Programme for Length 1996-1999). Replicas of these samples, and even replicas of the replicas can be produced (Daly, Ferguson, *et. al.* 1997). These samples are measured with a stylus instrument and mathematical techniques (similar to reversal methods) can be applied to extract the shape of the stylus. It is planned by NPL that the range of sinusoidal samples will be increased to include samples with multiple harmonics and varying phases. A number of comparisons of different instruments will then be carried out to assess the samples suitability as calibration artefacts. Watts, Sambles, *et. al.* (1997) have developed a method using surface plasmons to optically measure the shape of a stylus.

Scheer & Stover (1998) have developed square-wave gratings with depths in the range 1 to 10 nm. These samples are measured using AFM and angle resolved scatter (ARS) and power spectral analysis is used to correlate instruments with differing bandwidths. The production techniques stem from the silicon wafer technologies. Their route to traceability is via the laser source of the ARS instrument.

Haitjema (1998) has recently reported on a thorough investigation of the Form Talysurf stylus instrument. He suggests that deviations in comparisons are caused by short wavelength cut-offs due to stylus geometry and probe resonance oscillations. His method of calibration involves splitting the instrument into a number of sub-systems and using various metrological tools to calibrate the system as a whole. These separate measurements are described below:

x axis calibration

x axis calibration is required for the definition of the cut-off spatial wavelength, the sampling length and to calculate spacing and hybrid parameters (for example Δq). He uses a graduated rule and time-based analysis (this requires a constant traversing speed) to calibrate the *x* axis internal scales.

z axis calibration

Haijema has three methods for calibrating the *z* axis. Firstly, the stylus traces a standard sphere with known radius and the instrument calculates a polynomial correction for arcuate movement of the probe. Secondly, the length of a 0.5 mm gauge block wrung to a flat surface is measured and a length difference of around 10 μm is achieved by comparing two gauge blocks. The third method uses the set-up shown in figure 2.2. A piezoelectric actuator with capacitive feedback control (DPT) is connected to a function generator and used to move a small gauge block. The gauge block acts as a mirror for a differential plane mirror interferometer and as the contact point for the stylus. This is a very similar system to that of Bendeli, Duruz, *et. al.* (1974) except the traceability path is via the wavelength of the laser source as opposed to capacitance sensors. The same calibration procedures apply in both instruments.

Straightness datum

An optical flat (*Ra* ≈ 10 nm) is traced and the known profile minus the measured profile gives the noise. For more confidence in the measurements, the same part of the datum is used in a measurement of different parts of the flat.

Filter definition and dynamic probe behaviour

The frequency and amplitude of the vibrating gauge are varied and the dynamics of the system are investigated. The filtered and unfiltered data are compared plus the *Rq* measured with the Talysurf to the standard deviation measured with the interferometer system. From these data probe resonances can be identified as well as the effect of stylus flight.

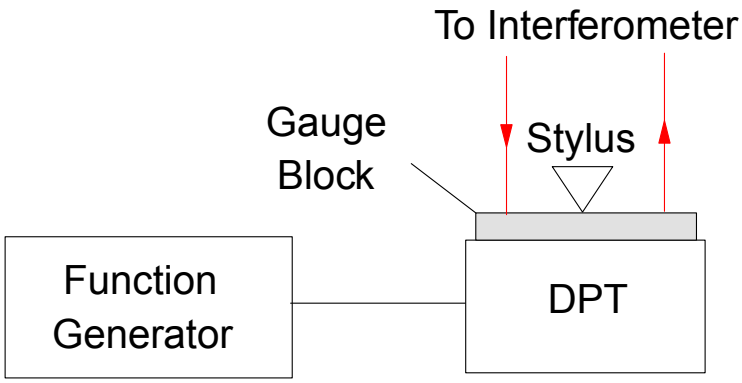

Figure 2.2 Vibrating stylus calibration rig, from Haitjema (1998)

Stylus geometry

The tip of an uncoated razor blade (< 0.1 μm tip radius) is measured and the stylus geometry calculated. Whitehouse (1994) also discusses using a razor blade to measure the stylus geometry plus an etched artefact with decreasing line-widths to measure geometry and wear.

Measuring force

For the static measuring force a mass balance is probed. Assuming that no stylus flight was apparent from the observations of the dynamic probe behaviour, the dynamic force will be less than the static force and is not measured. This assumption is not necessarily true (Liu, Chetwynd, *et. al.* 1993). The force is also checked as the direction of probing is reversed.

The above examples illustrate that traceability and calibration in surface texture measurement involves a multitude of artefacts and measurement strategies. The next section will examine the ISO standards that apply in the field.

3. STANDARDS

In 1994 Whitehouse listed over one hundred standards for surface texture measurement, but as more countries adopt the International Standards, this number has dropped to around fifty. There are, however, many more standards that relate to surface texture in some way. The following is a list of surface texture standards compiled using the 1998 Standards Infobase.

AGMA 118.01 (1995)	Information sheet - gear tooth surface texture for aerospace gearing (surface roughness, waviness, form and lay)
AS 2382 (1981)	Surface roughness comparison specimens
ASME B46.1 (1978)	Surface texture, (surface roughness, waviness and lay)
ASTM F 1048- (1992)	Test method for measuring the effective surface roughness of optical components by total integrated scatter
ASTM F 1438- (1997)	Test method for determining surface roughness by scanning tunneling microscopy for gas distribution system components
ASTM F 1811- (1997)	Practice for estimating the power spectral density function and related finish parameters from surface profile data
BS 1134: PT1 (1988)	Assessment of surface texture - methods and instrumentation
BS 1134: PT2 (1990)	Assessment of surface texture - guidance and general information
BS 2634: PT1 (1987)	Specification for roughness comparison specimens - specification for turned, ground, bored, milled, shaped and planed specimens
BS 2634: PT2 (1987)	Specification for roughness comparison specimens - specification for spark-eroded, shot blasted, grit-blasted and polished specimens
BS 6393 (1987)	As ISO 5436-
BS 6741: PT1 (1987)	Glossary of surface roughness terms - surface and its parameters
BS 6741: PT2 (1987)	Glossary of surface roughness terms - measurement of surface roughness parameters
BS 7900 (1998)	Specification for examination of surface texture of precision steel castings
BS ISO 3274 (1998)	As ISO 3274-
DD ENV 623 PT4 (1994)	Advanced technical ceramics - monolithic ceramics - general and textural properties - determination of surface roughness
DIN 31670 PT8 (1986)	Plain bearings: quality assurance of plain bearings: checking the geometrical tolerances and surface roughness of shafts, collars and thrust collars
DIN 31699 (1986)	Plain bearings: shafts, collars, thrust collars; geometrical tolerances and

	surface roughness
DIN 3969 PT1 (1991)	Surface roughness of tooth flanks; roughness parameters, surface grades
DIN 40686 SUPP2 (1983)	Surfaces of dense ceramic components for electrical engineering; determination of surface roughness
DIN 4762 (1981)	Surface roughness; terminology; surface & its parameters
DIN 4762 PT1 (1981)	Progressive ratio number values of surface roughness parameters
DIN 4766 PT1 (1981)	Surface roughness associated with types of manufacturing methods; attainable arithmetical mean value of peak-to-valley height Rz
DIN 4766 PT2 (1981)	Surface roughness associated with types of manufacturing methods; attainable arithmetical mean value Ra
DIN 4768 (1974)	Determination of values of surface roughness parameters Ra, Rz, Rmax using electrical contact (stylus) instruments; concepts and measuring conditions
DIN 4768 PT1 (1978)	Determination of surface roughness Ra, Rz, Rmax with electric stylus instruments; basic data
DIN 4772 (1979)	Electrical contact (stylus) instruments for measurement of surface roughness by profile method
DIN 4775 (1982)	Measuring of the surface roughness of workpieces; visual and tactile comparison, methods by means of contact stylus instruments
DIN 4776 (1990)	Determination of surface roughness parameters Rk, Rpk, Rvk, Mr1, Mr2 serving to decrease the material component of roughness profile
DIN 4776 SUPP1 (1990)	Measurement of surface roughness; parameters Rk, Rpk, Rvk, Mr1, Mr2 for description of material portion (profile bearing length ratio) in roughness profile; measuring conditions and evaluation procedures
DIN 54530 PT10 (1993)	Testing of paper and board cores; surface quality; determination of surface roughness and waviness
DIN V ENV 623 PT4	As DD ENV 623 PT4
ISO 1879-	Classification of instruments and devices for measurement and evaluation of the geometrical parameters of surface finish
ISO 1879- (1981)	Instruments for the measurement of surface roughness by the profile method - vocabulary
ISO 1880- (1979)	Instruments for the measurement of surface roughness by the profile method - contact (stylus) instruments of progressive profile transformation - profile recording instruments
ISO 3274- (1975)	Geometrical product specifications (GPS) - surface texture: profile method - nominal characteristics of contact (stylus) instruments
ISO 4287/1-(1984)	Surface roughness - terminology - surface and its parameters

ISO 4287/2- (1984)	Surface roughness - terminology - measurement of surface roughness parameters
ISO 4288- (1983)	Geometrical product specifications (GPS) - surface texture: profile method - rules and procedures for the assessment of surface texture
ISO 468- (1972)	Surface roughness - parameters, their values and general rules for specifying requirements
ISO 5436- (1985)	Calibration specimens - stylus instruments - types, calibration and use of specimens
JIS-B0601 (1982)	Surface roughness - definitions and designation
JIS-B0652 (1973)	Instruments for the measurement of surface roughness by the interferometric method
JIS-K7104 (1976)	Methods for comparison of surface roughness of plastics
MIL-I-45177 (1996)	Instrument, tracer, surface roughness
NAS 30 (1956)	Surface roughness designation
NAS 31 (1958)	Conversion table, surface roughness designations
SIS 81 20 05 (1973)	Concrete surfaces. Determination of surface roughness
SS 674 (1989)	Surface roughness - guidance for the choice of surface roughness
SS 675 (1989)	Surface roughness - measurement of surface roughness by means of electrical profile recording instruments
SS ENV 623-4	As DD ENV 623 PT4
SS ISO 4287-1	As ISO 4287/1-
SS ISO 4287-2	As ISO 4287/2-
SS ISO 4288 (1988)	Rules and procedures for the measurement of surface roughness using stylus instruments
SS ISO 468	As ISO 468-
UNI ISO 1879	As ISO 1879-
UNI ISO 1880	As ISO 1880-
UNI ISO 4287/1	As ISO 4287/1-
UNI ISO 4287/2	As ISO 4287/2-
UNI ISO 4288	As SS ISO 4288
UNI ISO 468	As ISO 468-
VD/VDE 2615 (1988)	Surface roughness measurement of cylindrical gears and bevel gears by means of electrical stylus-type instruments

The most important standard as far as this report is concerned is ISO 5436 (1985*): Calibration specimens - stylus instruments - types, calibration and use of specimens*. This standard advocates the use

of calibration specimens or artefacts to calibrate the operating characteristics of contact stylus instruments. Four different types of specimen are described:

Type A - These are used to measure the vertical magnification of an instrument. They come in two sub-groups: *Type A1* - a wide calibrated groove with a flat valley the size of which is dictated by the dimensions of the stylus tip, *Type A2* - same as A1 but with a rounded valley.

Type B - These are used to investigate the geometry of the stylus tip. They also come with two sub-groups: *Type B1* - narrow grooves proportioned to be sensitive to the dimensions of the stylus; *Type B2* - two grids of equal *Ra*, one sensitive to the tip dimensions the other insensitive.

Type C - These are used to check parameter meters. They consist of a grid of repetitive grooves of similar shape (for example sinusoidal, triangular and arcuate waveforms) with low harmonic amplitudes. Type C specimens have well documented surface texture parameters and can be used to check the horizontal magnification.

Type D - These are used for an overall check of the meter calibration. They have irregular profiles in the direction of traverse, but they have the convenience of an approximately constant cross-section along their lengths.

All the specimens are made of suitably hard materials but glass or quartz is favoured. At the time of writing the type B1 specimens are still under development.

Calibration of the specimens is carried out using interferometry and the route to traceability is via the calibrated vacuum wavelength of the source. The use of interferometry usually requires the surface to be metalised and only shallow grooves can be measured without having to resort to specialised fringe analysis techniques. Problems arise due to the differences between the interaction of a contact stylus instrument and the surface and an optical beam and the surface. Examples quoted in the standard are the effects of the optical properties of the specimen material and the effects of oblique incidence. The magnitude of these effects is assumed negligible by the standard - a assumption that is not considered wise by the author.

ISO 5436 goes on to consider the calibration aspects of instruments with a datum skid, the effects of stylus wear, practical use of the standard specimen and error statements. Very little, if any, real consideration is given to the statement of uncertainty that would either accompany a calibrated

instrument or the artefacts used to calibrate an instrument. This is thought to be an aspect of the standards that is not sufficiently covered.

4. A FULLY TRACEABLE INSTRUMENT: NANOSURF IV

NanoSurf IV is a surface texture measuring instrument that measures displacements in two nominally orthogonal axes with an uncertainty of better than 1 nm. Many instruments can resolve sub-nanometre features but the user has no way of knowing whether the readout of the co-ordinates from the instrument is correct. They are fiducial indicators - not measuring instruments in the true sense of the word. NanoSurf IV is simply a stylus instrument but with traceable metrology inherent in its design. Figure 4.1 shows the subsystems of NanoSurf IV and illustrates how they are related. In addition to the core subsystems there is also instrumentation to input the signals from the interferometers and control the moving parts in the instrument, a computing system that automates a measurement and carries out any data analysis, plus systems to control the environment in which the instrument is housed. Each is described in detail elsewhere (Leach 2000). Figure 4.2 is a photograph of NanoSurf IV with only the electronic and computer subsystems not shown.

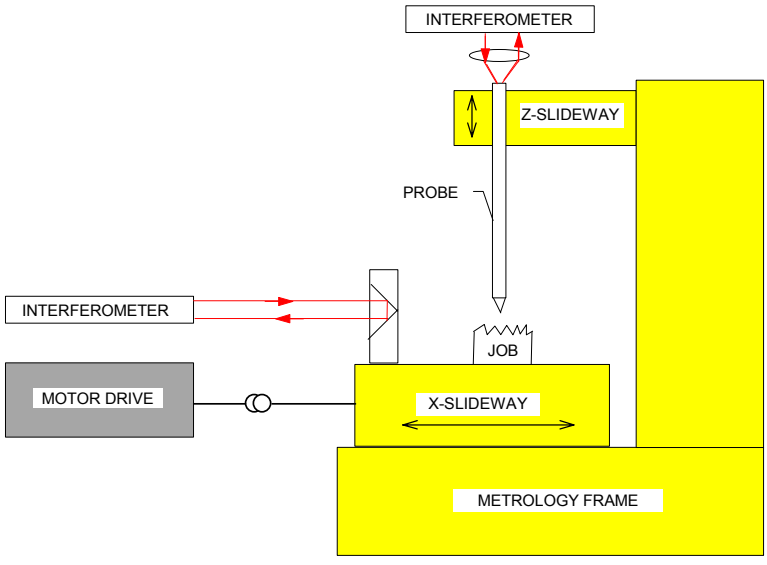

Figure 4.1 Schema of NanoSurf IV

Briefly, with reference to figure 4.1, the object to be measured is placed on a specimen table that in turn sits on the *x* slideway. The *z* slideway is used to bring the stylus into contact with the surface to be measured. The drive mechanism pushes or pulls the *x* slideway via a coupling rod and hence

moves the surface being measured whilst the stylus follows the surface. The displacements in the x and z axes are measured using two non-polarising Michelson interferometers.

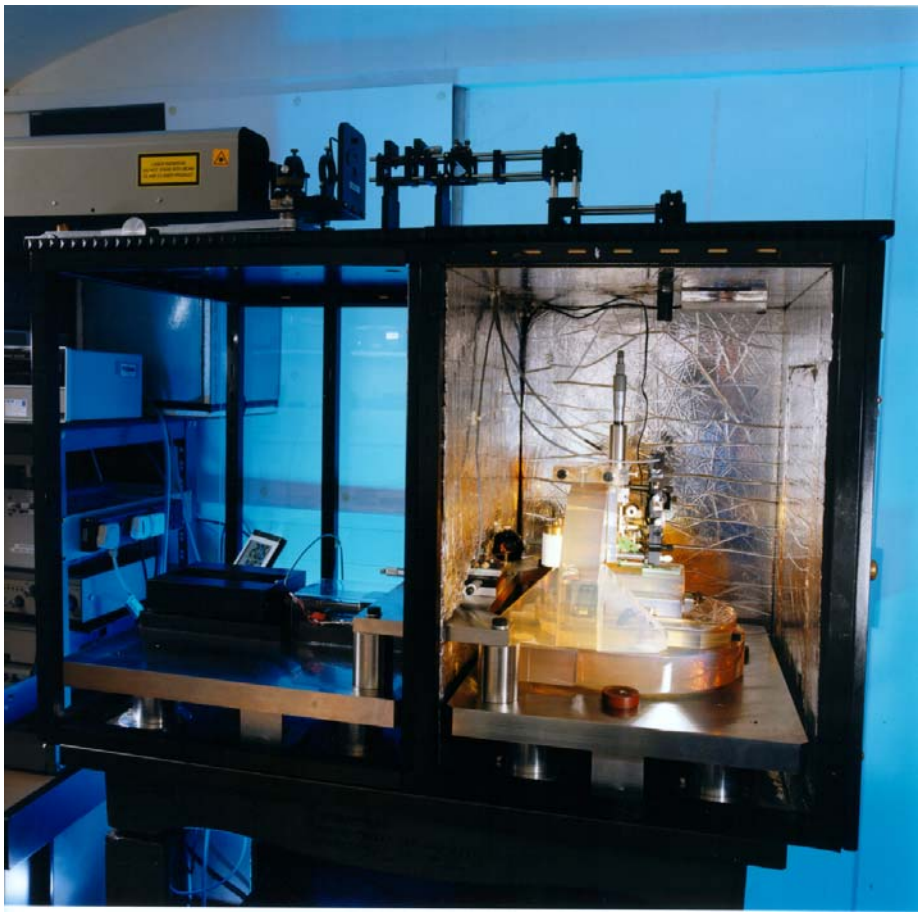

Figure 4.2 The sub-systems of NanoSurf IV

5. UNCERTAINTY ANALYSIS OF NANOSURF IV

The uncertainty analysis of NanoSurf IV has been split into two sections. Firstly, the uncertainty of a length measurement made using the interferometers and secondly the uncertainty in a measurement of a surface roughness parameter. At all times the uncertainty calculation follows internationally accepted guidelines for the evaluation and expression of uncertainties as laid out in the *Guide to the Expression of Uncertainty in Measurement* (1993), herein simply referred to as the *GUM*.

5.1 COMBINED STANDARD UNCERTAINTY

The combined standard uncertainty, $u_c(L)$ is an estimate of the standard deviation of the distribution of possible values (or probability distribution) of a length measurement made using an interferometer, L. The combined standard uncertainty, as its name implies, is a quadrature sum of the uncertainties $u(x_i)$ of all the influence factors x_i, weighted by a sensitivity coefficient [§5.1.2 *GUM*]

$$u_c{}^2(L) = \sum_{i=1}^{N} c_i{}^2 u^2(x_i) + \sum_{i=1}^{N} \sum_{j=1}^{N} \left[\frac{1}{2} c_{ij}{}^2 + c_i c_{ijj} \right] u^2(x_i) u^2(x_j) \tag{5.1}$$

where $u(x_i)$ are the standard uncertainties attributed to the influence quantities x_i, and where the sensitivity coefficients

$$c_i = \frac{\partial L}{\partial x_i}, \; c_{ij} = \frac{\partial^2 L}{\partial x_i \partial x_j}, \; c_{ijj} = \frac{\partial^3 L}{\partial x_i \partial^2 x_j} \tag{5.2}$$

are the partial derivatives of the model equation. Note that equation (5.1) assumes the input quantities are uncorrelated and is only an approximation of the uncertainty.

It is convenient to think of equation (5.1) as consisting of two parts: terms containing $u^2(x_i)$, and cross terms containing $u^2(x_i)u^2(x_j)$ that take into account the degree of non-linearity in the model. The cross terms may be referred to as second order terms by some authors in the literature, including the *GUM*.

5.2 TYPE A AND TYPE B UNCERTAINTIES COMPONENTS

In the *GUM* there is considerable concern about distinguishing between Type A and Type B uncertainty components. The distinction between Type A and Type B uncertainties relates to the manner in which they are established and not how they are subsequently treated when they are combined. Type A uncertainties are those for which repeated measurements are made and the standard deviation is evaluated from the data, and used as the standard uncertainty. Type B uncertainties are those for which repeated measurements cannot simply isolate the influence, and the uncertainty must be referred to by some other means [§4.2, §4.3 *GUM*].

The rectangular distribution occurs in Type B uncertainty evaluation and is used frequently in this section. As explained in §4.4.5 of the *GUM*, if data to estimate the uncertainty distribution of an influence parameter are limited, often an adequate and useful approximation is to assume an upper $+a$ and a lower $-a$ bound for a range of equally probable values. The standard uncertainty (§4.3.7 *GUM*) is then given by $a/\sqrt{3}$. Similarly, a reading from a meter read-out of resolution b has a standard uncertainty of $b/\sqrt{12}$ [§F.2.2.1 *GUM*]; the reading is considered to be a rectangular distribution bounded by $\pm a = +b/2$ and $-b/2$.

5.3 DEGREES OF FREEDOM

The degrees of freedom, ν_{x_i} are estimated for each of the $u(x_i)$. For Type A uncertainty evaluation, the degrees of freedom $\nu = n - 1$, where n is the number of observations taken to determine the arithmetic mean [§G.3.3 *GUM*]. In many cases, the uncertainty evaluation is Type B, and the degrees of freedom are estimated according to the relative uncertainty in the uncertainty $\Delta u/u$, or to put it another way - the judgement of reliability or confidence in the estimation of the uncertainty is given by [§G.4.2 *G UM*]

$$\nu_i \approx \frac{1}{2}\left[\frac{\Delta u(x_i)}{u(x_i)}\right]^{-2}. \qquad (5.3)$$

Degrees of freedom for influence parameter uncertainties are combined in one step for the overall uncertainty budget effective degrees of freedom, by applying the Welch-Satterthwaite formula [§G.4.1 *GUM*]

$$\nu_{eff} = \frac{u_c^4(y)}{\sum_{i=1}^{N} \frac{u_i^4(y)}{\nu_i}}. \tag{5.4}$$

Degrees of freedom are always truncated to the next integer [§G.4.1 *GUM*].

5.4 EXPANDED UNCERTAINTY

It is desirable to express uncertainties so that for most of the measurements the measured value is within the uncertainty range of the 'true value'. The expanded uncertainty [§6.2 *GUM*]

$$U = ku_c(L) \tag{5.5}$$

is defined as the combined uncertainty multiplied by a coverage factor k. The value of the coverage factor is chosen depending on the level of confidence that would facilitate the interpretation of the uncertainty and the number of degrees of freedom. Most measurements are expressed with a value of k between two and three. k = 2 corresponds to a confidence level of approximately 95% assuming a high number of degrees of freedom [§6.2.2 *GUM*].

The steps involved in this uncertainty analysis are based upon those presented by Decker, Ulrich, *el. al.* (1998):

Step 1: Analyse the measurement process and identify the influence quantities.
Step 2: List any simplifying assumptions and their impact on the measurement.
Step 3: Form a mathematical model of the measurement in terms of the influence quantities (expressed in an optimal form).
Step 4: Evaluate the sensitivity coefficients of the influence quantities.
Step 5: Evaluate the standard uncertainties and degrees of freedom of the influence quantities.
Step 6: Determine correlated components.

Step 7: Calculate the combined and expanded uncertainties and degrees of freedom for the overall process.

5.5 MEASUREMENT PROCESS

At this stage only the displacement of either the cat's-eye in the z axis or the corner-cube in the x axis is analysed. The following influence quantities are considered:

Laser source:

- short and long-term calibration;
- frequency stability;
- intensity stability;
- beam characteristics;
- polarisation.

Interferometer characteristics:

- collimation/obliquity effects;
- quality of the optical components;
- air refractive index ;
- stray beams;
- diffraction effects;
- dead path error;
- air turbulence effects.

Metrology frame:

- thermal expansion;
- mechanical expansion and rigidity;
- Abbe offset;
- cosine error;
- co-ordinate orthogonality.

Detection system:

- linearity of photo-detectors;

- detector geometry;
- electronic noise;
- frequency response;
- resolution.

Computing/software:

- quality of mathematical fits and models.

By identifying the specific characteristics of the measurement procedure and considering the conditions of the laboratory, some of these influence quantities can be combined or be deemed negligible. When an influence quantity is deemed negligible it is because sound physical laws have been applied to model its magnitude and effect, or because it has been measured to be negligible. It is important to appreciate that the final uncertainty in length measurement is for a strict range of conditions and techniques.

5.6 ASSUMPTIONS

Evaluation of measurement uncertainty must be for a specific measurement scenario. The specifics of the measurement and the influence factors should be well defined before trying to consider their uncertainties. At this stage their are no simplifying assumptions apparent to the NanoSurf IV measurement technique. Of course, the assumption is made that operators of NanoSurf IV are applying best laboratory practice that is free of blunders. The ISO 9001 Quality Management System in operation at NPL should ensure this.

5.7 MATHEMATICAL MODEL OF THE MEASUREMENT

The primary influence factors recognised above can be expressed algebraically and combined to yield a mathematical model representing the measurement. Starting from first principles the measured displacement of one of the retro-reflectors in an ideal Michelson interferometer is given by

$$L_\phi = \frac{\lambda}{2\pi}\Delta\phi \tag{5.6}$$

where λ is the wavelength of the laser source and $\Delta\phi$ is the difference in the phase from the reference and measurement arms of the interferometer. A non-ideal interferometer will measure a length given by

$$L = L_\phi + L_\Omega + L_n + L_t + L_m + L_A + L_d + L_T + L_j \tag{5.7}$$

where L_Ω is a correction to the measured length for the effects of diffraction, L_n is a correction due to the change in the refractive index of the air in which the laser operates, L_t is that for thermal effects on the metrology frame, L_m is that for mechanical effects on the metrology frame, L_A is that for the imperfect optics and stray beams, L_d is that for the dead path length, L_T is that for the effects of air turbulence and L_j is that for the measurement set-up, *i.e.* Abbe and cosine errors. Once again, it assumed that the input quantities are uncorrelated.

5.8 EVALUATION OF THE SENSITIVITY COEFFICIENTS

The equation for the combined standard uncertainty is applied to the mathematical model describing the measurement. Simply making the substitution of the influence variables in place of the x_i in equation (5.1), the combined standard uncertainty can be written as

$$\begin{aligned} u_c^2(L) = {} & c_{L_\phi}^2 u^2(L_\phi) + c_{L_\Omega}^2 u^2(L_\Omega) + c_{L_n}^2 u^2(L_n) + c_{L_t}^2 u^2(L_t) + c_{L_m}^2 u^2(L_m) + c_{L_A}^2 u^2(L_A) \\ & + c_{L_d}^2 u^2(L_d) + c_{L_T}^2 u^2(L_T) + c_{L_j}^2 u^2(L_j) + \text{higher order terms} \end{aligned} \tag{5.8}$$

where the sensitivity coefficients, c_i, for the first order terms are

$$\begin{aligned} & c_{L_\phi} = \frac{\partial L}{\partial L_\phi},\ c_{L_\Omega} = \frac{\partial L}{\partial L_\Omega},\ c_{L_n} = \frac{\partial L}{\partial L_n},\ c_{L_t} = \frac{\partial L}{\partial L_t},\ c_{L_m} = \frac{\partial L}{\partial L_m},\ c_{L_A} = \frac{\partial L}{\partial L_A},\ c_{L_d} = \frac{\partial L}{\partial L_d}, \\ & c_{L_T} = \frac{\partial L}{\partial L_T},\ c_{L_j} = \frac{\partial L}{\partial L_j}. \end{aligned} \tag{5.9}$$

Calculating the partial derivatives c_i, c_{ij} and c_{ijj} in equation (5.8) determines the sensitivity coefficients for the uncertainty in displacement measurement. In the case of equation (5.8) all of the first order terms are equal to unity and the higher order terms are equal to zero. Each term in equation (5.8) is now examined in detail.

5.9 STANDARD UNCERTAINTIES OF INFLUENCE QUANTITIES

5.9.1 Optical path difference

The combined uncertainty in the measurement of the optical path difference is given by

$$u_c^2(L_\phi) = c_{\Delta\phi}^2 u^2(\Delta\phi) + c_\lambda^2 u^2(\lambda) + \text{higher order terms.} \qquad (5.10)$$

The first order sensitivity coefficients are given by $(\lambda/2\pi)$ and $(\Delta\phi/2\pi)$ respectively. For convenience, c_λ is expressed as L/λ. The second-order nature of the all higher order coefficients means they are negligible.

5.9.2 Measured parameters influencing the measurement of the optical path difference

Vacuum wavelength

The laser wavelength is calibrated by beat frequency measurement against one of the standard NPL iodine-stabilised lasers. The wavelength stability is quoted as ± 1 x 10^{-9} over 24 hours with a drift of ± 1 x 10^{-8} between calibrations (every 2500 hours). Table 5.1 shows the uncertainty contributions.

Source	Size	k	Standard uncertainty	Sensitivity coefficient	Contribution
Primary laser accuracy	2.5 x 10^{-11} λ	1	2.5 x 10^{-11} λ	L/λ	2.5 x 10^{-11} L
Stability of laser	1 x 10^{-9} λ	1	1 x 10^{-9} λ	L/λ	1 x 10^{-9} L
Yearly drift range	1 x 10^{-8} λ	1	1 x 10^{-8} λ	L/λ	1 x 10^{-8} L
					1 x 10^{-8} L

Table 5.1 Summation of uncertainties due to the laser source

Phase difference

The uncertainty in the phase difference measurement cannot easily be differentiated from other sources of uncertainty. Its effect is measured in §5.9.4 and summarised in table 5.2. Notice that the effect of this uncertainty is considered twice in the uncertainty analysis - once in combination with the calibration parameters of the laser wavelength and again in §5.12 as a purely random and experimentally determined parameter.

Source	Size	k	Standard uncertainty	Sensitivity coefficient	Contribution
Random phase fluctuation	0.1 nm	1	0.1 nm	1	0.1 nm
					0.1 nm

Table 5.2 Summation of uncertainties due to fluctuations in the phase measurement

5.9.3 Overall uncertainty due to the measured optical path difference

Combining the values for the sensitivity coefficient and the measured parameters gives a total uncertainty in the measurement of the optical path difference of

$$u_c(L_\phi) = \sqrt{(1\times10^{-2}\,L)^2 + 0.01}\ \text{nm} \tag{5.11}$$

where L is in millimetres.

5.10 DIFFRACTION EFFECTS AND MISALIGNMENT

As the interferometers are illuminated by a laser source, the shift of the phase and changes in the curvature of the wavefronts lead to systematic errors, to which there must be added the error caused by misalignments. Consider an ideal interferometer illuminated by a monochromatic Gaussian beam that produces two interfering beams. No diffraction is assumed to occur in the optical system. The error in the fringe spacing when the interference pattern is focussed onto the detector is given by (Mana 1989)

$$\frac{2\Delta\lambda_0}{\lambda} = \left(\frac{1}{k^2 {w_0}^2}\right)\left(\frac{\left[1 + 2u^2 / {w_f}^2\right]e^{-2u^u/{w_f}^2} - 1}{e^{-2u^u/{w_f}^2} - 1}\right) + \left(\frac{2}{k^2 {w_0}^2}\right)\left(\frac{b}{2D}\right)^2 \tag{5.12}$$

where λ is the wavelength of the laser source, λ_0 is the fringe displacement, k is the wavenumber, w_0 is the waist of the laser, u is the aperture radius, D is the absolute distance of the lens from the waist of the beam, f is the focal length of the lens and w_f and b are given by

$$w_f = 2\left(\frac{f}{b}\right)w_0 \tag{5.13}$$

and

$$b = k{w_0}^2 . \tag{5.14}$$

Before calculating the error term given by equation (5.12) it is necessary to calculate the effective beam waist due to the collimating telescope. To do this a new waist is found for each of the optical elements by using the following (Self 1983)

$$\frac{1}{f} = \frac{1}{s''} + \frac{1}{s + {z_R}^2/(s - f)} \tag{5.15}$$

and

$${z_R}'' = m^2 z_R \tag{5.16}$$

where s is the object to lens distance, s'' is the image to lens distance, m is the magnification and z_R is the Rayleigh length or the distance over which the beam radius spreads by a factor of √2. The Rayleigh length is related to the beam waist by

$$z_R = \frac{\pi {w_0}^2}{\lambda} . \tag{5.17}$$

From the numerical values of the interferometer systems, $\Delta\lambda$ turns out to be less than 30 fm and is considered negligible.

Assuming the size of the detector is a lot larger than the spot size and that

$$\frac{\alpha}{\theta} \leq \frac{z}{|z-l|} \tag{5.18}$$

where α is the misalignment angle, l is the distance between the waist and the retro-reflector, z is the distance between the waist and the detector, $\theta = \lambda/(\pi w_0)$, the normalised error can be reduced to

$$\frac{4}{\theta^2}\frac{2\Delta\lambda_0}{\lambda} = 1 - \left(\frac{v^2-2}{8v^2}\right)\sigma^2. \tag{5.19}$$

In equation (5.19) $v = w/w_o$, $\sigma = 2\alpha/(v\theta)$ and

$$w^2 = w_0{}^2\left[1 + 4(z/b)^2\right]. \tag{5.20}$$

Inserting values for the parameters in equation (5.19), even if the interferometer were misaligned by as much as α = 5 °, $\Delta\lambda$ would only be equal to 0.1 pm. This source of uncertainty is, therefore, taken to be negligible.

According to the above the correction for the effects of diffraction and misalignment of the interferometer, L_Ω = 0, as are its associated uncertainties.

5.11 AIR REFRACTIVE INDEX

When performing optical interferometry in air, it is important to correct the laser wavelength for the refractivity of the air through which it passes. The correction factor, the refractive index, is applied to the vacuum wavelength of the light emitted by the laser

$$\lambda = \frac{\lambda_{vac}}{n} \tag{5.21}$$

where λ_{vac} is the wavelength in vacuum and n is the refractive index of air, for ambient conditions.

5.11.1 Equations for the refractivity of air

In 1965 Edlén reviewed the most recent work, collated findings and issued new formulae for the dispersion of air. The formulae derived in that paper have since been widely used to correct for the refractivity of air, with a minor correction to the humidity term suggested by Birch & Downs (1988) and a further correction suggested by Bönsch and Potulski (1998) for the latest standard conditions. The calculation starts with the dispersion of dry air for the new standard conditions, temperature t = 20 °C (ITS-90), pressure p = 100 000 Pa and 0.04% carbon dioxide content, describing the refractivity of standard air dependent on the wavenumber $\sigma = 1/\lambda$.

$$(n-1)_N .10^8 = 8091.37 + \frac{233\ 3983}{130-\sigma^2} + \frac{15\ 518}{38.9-\sigma^2}. \tag{5.22}$$

A CO_2 content x, differing from 0.04%, changes the refractivity to

$$(n-1)_x = (n-1)_N \left[1 + 0.5327(x - 0.0004)\right]. \tag{5.23}$$

The deviation of temperature and pressure from the reference conditions is taken into account by

$$(n-1)_{tp} = \frac{(n-1)_x\, p}{93214.6} \frac{1 + 10^{-8}(0.5953 - 0.009876t)p}{1 + 0.003661t}. \tag{5.24}$$

The influence of water vapour with partial pressure f is calculated, which results in the refractive index for moist air

$$n_{tpf} - n_{tp} = -f\left(3.802 - 0.0384\sigma^2\right).10^{-10}. \tag{5.25}$$

The uncertainty attributed to the empirical determination of the numerical coefficients in this equation ± 1×10^{-8} at the one standard deviation level of confidence (Birch & Downs 1994).

The length correction that accounts for the refractive index of air is given by

$$L_n = -nL \tag{5.26}$$

and its combined standard uncertainty

$$\begin{aligned} u_c^{\,2}(L_n) = &\left(\frac{\partial L_n}{\partial p}\right)^2 u_c^{\,2}(p) + \left(\frac{\partial L_n}{\partial x}\right)^2 u_c^{\,2}(x) + \left(\frac{\partial L_n}{\partial t}\right)^2 u_c^{\,2}(t) + \left(\frac{\partial L_n}{\partial f}\right)^2 u_c^{\,2}(f) \\ &+ \left(\frac{\partial L_n}{\partial \lambda}\right)^2 u_c^{\,2}(\lambda) + \text{higher order terms} \end{aligned} \quad . \tag{5.27}$$

Calculating the partial derivatives and putting in the values of the reference conditions the sensitivity coefficients are given by (see §5.11.2 for the reference values of humidity)

$$\begin{aligned} \left(\frac{\partial L_n}{\partial p}\right) &= 2.68 \times 10^{-9}\, L \text{ / Pa} \\ \left(\frac{\partial L_n}{\partial x}\right) &= 1.4 \times 10^{-10}\, L \text{ / ppm} \\ \left(\frac{\partial L_n}{\partial t}\right) &= -9.30 \times 10^{-7}\, L/^\circ\text{C}\,. \\ \left(\frac{\partial L_n}{\partial f}\right) &= -3.8 \times 10^{-10}\, L \text{ / Pa} \\ \left(\frac{\partial L_n}{\partial \lambda}\right) &= 1.22 \times 10^{-5}\, L \text{ / } \mu\text{m} \end{aligned} \tag{5.28}$$

The largest cross term is given by

$$\frac{1}{2} c_{tt}^{\,2} + c_t c_{ttt} = 8 \times 10^{-9}\, L^2 \text{ / } ^\circ\text{C}^2, \tag{5.29}$$

but this would multiply $u^2(x_t)$ and it is therefore considered that all cross terms are negligible.

5.11.2 Conversion of humidity units

The humidity is measured using a dewpoint hygrometer, which displays results in the form of °C dewpoint temperature. Magnus' relation (BS 1339: 1965) is used to convert °C dewpoint into partial pressure of water vapour for use by the Edlén equations and is given by

$$f = 10^{\left(0.7857+\frac{7.5t_{dp}}{237.3+t_{dp}}\right)} \tag{5.30}$$

where t_{dp} is the dewpoint temperature in ^{o}C. Partially differentiating gives

$$\left(\frac{\partial f}{\partial t_{dp}}\right) = \ln(10) \times \left[\frac{-7.5t_{dp}}{\left(237.3+t_{dp}\right)^{2}} + \frac{7.5}{237.3+t_{dp}}\right] \times 10^{\left(0.7857+\frac{7.5t_{dp}}{237.3+t_{dp}}\right)}. \tag{5.31}$$

In most dimensional metrology laboratories the humidity is controlled at around 10 ^{o}C dewpoint. Substituting t_{dp} = 10 ^{o}C gives

$$\left(\frac{\partial f}{\partial t_{dp}}\right) = 82.2\,\text{Pa}\ {}^{o}\text{C}^{-1}. \tag{5.32}$$

Hence a variation in humidity of 1 ^{o}C dewpoint alters the partial pressure by 82.2 Pa and hence the refractive index by 3.12 x 10^{-8}.

5.11.3 Measured parameters influencing the refractive index of air

Air temperature

The air temperature is measured by platinum resistance thermometers (PRTs) inside the anechoic chamber and close to the object being measured. The calibration certificate of the PRTs states a calibration uncertainty of ± 0.005 ^{o}C at a 95% confidence level. The self-heating of the PRT (Downs, Ferris, *et. al.* 1990) was assessed by observing a typical PRT resistance reading as the current was increased by a factor of √2 from its initial value of 1 mA. Table 5.3 summarises the contributions due to the air temperature measurement.

Air pressure

The pressure transducer is located inside the equipment rack and is connected to the anechoic chamber via PVC tubing. The calibration certificate quotes an uncertainty of ± 5 Pa at a confidence

level of 95% for the primary standard, and shows a variation of ± 20 Pa in calibrated results. Table 5.4 summarises the contributions due to the measurement of air pressure.

Source	Size	k	Standard uncertainty	Sensitivity coefficient	Contribution
Resistance bridge accuracy	3 mK	√3	1.7 mK	9.30 x 10^{-7} L/K	1.6 x 10^{-9} L
PRT calibration	5 mK	1.96	2.6 mK	9.30 x 10^{-7} L/K	2.4 x 10^{-9} L
ITS90 equations	0.13 mK	1	0.13 mK	9.30 x 10^{-7} L/K	1.2 x 10^{-10} L
PRT inter-calibration drift	2 mK	1	2 mK	9.30 x 10^{-7} L/K	1.9 x 10^{-9} L
PRT - air lag	10 mK	√3	5.8 mK	9.30 x 10^{-7} L/K	5.4 x 10^{-9} L
Self heating of PRT	12 mK	√3	6.9 mK	9.30 x 10^{-7} L/K	6.4 x 10^{-9} L
					9.1 x 10^{-9} L

Table 5.3 Summation of uncertainties due to air temperature measurement

Source	Size	k	Standard uncertainty	Sensitivity coefficient	Contribution
Primary standard uncertainty	5 Pa	1.96	2.6 Pa	2.68 x 10^{-9} L/Pa	7.0 x 10^{-9} L
Sensor variability	20 Pa	√3	11.6 Pa	2.68 x 10^{-9} L/Pa	3.1 x 10^{-8} L
Sensor resolution	1 Pa	√12	0.3 Pa	2.68 x 10^{-9} L/Pa	8.0 x 10^{-10} L
					3.2 x 10^{-8} L

Table 5.4 Summation of uncertainties due to air pressure measurement

Humidity

The humidity transducer is located inside the equipment rack and is connected to the anechoic chamber via PVC tubing. The calibration certificate quotes an uncertainty of ± 0.2 °C at a confidence level of 95%. Table 5.5 summarises the contributions due to the measurement of humidity.

Source	Size	*k*	Standard uncertainty	Sensitivity coefficient	Contribution
Dewpoint meter calibration	0.2 °C DP	1.96	0.10 °C DP	3.0×10^{-8} *L*/°C DP	3.0×10^{-9} *L*
Magnus' equation	0.2 °C DP	√3	0.12 °C DP	3.0×10^{-8} *L*/°C DP	3.6×10^{-9} *L*
Interface resolution	0.5 °C DP	√12	0.14 °C DP	3.0×10^{-8} *L*/°C DP	4.2×10^{-9} *L*
					6.3×10^{-9} *L*

Table 5.5 Summation of uncertainties due to air humidity measurement where DP = Dewpoint temperature

Carbon dioxide content

Typical changes in the carbon dioxide content in a laboratory, due to such things as human respiration, can be up to 100 ppm (Downs 1998). Table 5.6 shows the effect of this departure on the uncertainty due to the refractive index.

Source	Size	k	Standard uncertainty	Sensitivity coefficient	Contribution
Departure from standard conditions (*i.e.* 400 ppm)	100 ppm	1	100 ppm	1.47×10^{-10} *L*/ppm	1.47×10^{-8} *L*
					1.47×10^{-8} *L*

Table 5.6 Summation of uncertainties due to air carbon dioxide content

Vacuum wavelength

The combined uncertainty attributed to the vacuum wavelength through its contribution to the refractive index of air is very small. Using values from table 5.1 and equation (5.28) gives

$$u_c(\lambda) = 8 \times 10^{-14}\, L \tag{5.33}$$

which is considered negligible.

Uncertainty of the Edlén equations

Table 5.7 presents the contribution due to the uncertainty in the Edlén equations.

Source	Size	k	Standard uncertainty	Sensitivity coefficient	Contribution
Accuracy of Edlén equations	3×10^{-8}	3	1×10^{-8}	L	$1.0 \times 10^{-8}\, L$
					$1.0 \times 10^{-8}\, L$

Table 5.7 Summation of uncertainties due to the Edlén equations

5.11.4 Overall uncertainty due to the refractive index of air measurement

Combining the values for the sensitivity coefficients and the measured parameters gives a total uncertainty in the refractive index measurement of

$$u_c(L_n) = 3.8 \times 10^{-8}\, L \tag{5.34}$$

where L is the measured length.

5.12 EFFECTS ON THE METROLOGY FRAME AND DETECTOR ELECTRONICS

It is very difficult to separate the effects of thermal and mechanical changes on the metrology frame plus the effects of the detector electronics and data processing. It is also very difficult to rigorously model these effects. For these reasons, the stability of the metrology frame, detection

system and mathematical algorithms has been experimentally measured with no regard as to the source of any fluctuations, *i.e.* a correction for the stability of the metrology frame and detection system is equal to ($L_t + L_m + L_T + L_\phi$). It must also be remembered that other random uncertainty contributions, such as refractive index fluctuations, will also be present in these measurements. The measured uncertainty term is, therefore, expected to be a pessimistic value.

To measure the stability of the metrology frame and detection system, the output of the interferometers was monitored over a one minute period with the retro-reflectors stationary. The results are given in table 5.8. During the experiments the humidity and barometric pressure were monitored for stability - any noticeable drift or large fluctuations voided the experiment.

Source	Size	k	Standard uncertainty	Sensitivity coefficient	Contribution
x axis dimensional change	0.1 nm	1	0.1 nm	1	0.1 nm
					0.1 nm

Table 5.8 Summation of uncertainties due to dimensional fluctuations of the metrology frame

5.13 EFFECTS OF IMPERFECT OPTICS AND STRAY BEAMS

Due to the very high spatial and temporal coherence of the laser source, stray light can interfere with beams reflected from the surfaces present in reference and measurement arms of the interferometers. The dominant effects are usually due to unwanted reflections and isolated strong point scatterers, both leading to random and non-random spatial variations in the scattered phase and amplitude (Hariharan 1997). This analysis does not attempt to isolate sources of stray reflection.

Assuming the stray light affects one beam only, its amplitude, a_s, adds vectorily to the amplitude of the main beam, a as in figure 5.1.

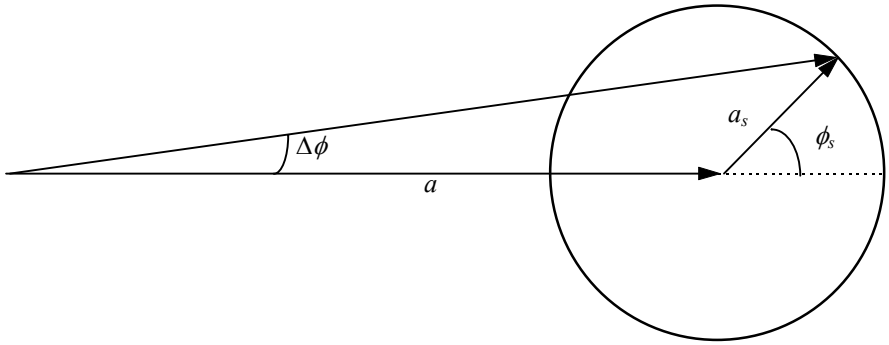

Figure 5.1 Phase shift of a beam produced by coherent stray light that has travelled an additional path

In the case of a Michelson interferometer, the complex amplitude at any point in the interference pattern is obtained by summing the complex amplitude of the stray light and the complex amplitudes of the beams reflected from the reference and test surfaces. If we assume that the beams reflected from the reference and test surfaces have unity intensity, the resultant complex amplitude is given by the relation

$$a(x,y) = \left|1 + e^{[-i\phi(x,y)]} + a_s(x,y)e^{[-i\phi_s(x,y)]}\right| \tag{5.35}$$

where $\phi_s = (2\pi/\lambda)p$, and p is the difference in the lengths of the optical paths traversed by the stray light and by the test beams relative to the beam reflected from the reference surface. The intensity in the interference pattern is then

$$I(x,y) = a^2(x,y) = 2 + \left|a_s\right|^2 + 2a_s\cos\phi_s + 2\left[1 + a_s\cos\phi_s\right]\cos\phi + 2a_s\sin\phi_s\sin\phi\,. \tag{5.36}$$

Assuming $a_s \approx 1$, $\Delta\phi$ can be found by equating the following

$$\left[1 + a_s\cos\phi_s\right]\cos\phi + a_s\sin\phi_s\sin\phi \equiv A\cos(\phi - \Delta\phi)\,. \tag{5.37}$$

After some simple trigonometry and assuming $\Delta\phi$ is a small angle the magnitude of the phase error is given by

$$\Delta\phi \approx a_s\sin\phi_s\,. \tag{5.38}$$

To minimise the effects of stray reflections all the optical components are thoroughly cleaned, the retro-reflectors are mounted at a non-orthogonal angle to the beam propagation direction (to avoid reflections off the front surfaces) and all the non-critical optical surfaces are anti-reflection (AR) coated. It is extremely difficult, if not impossible, to measure the amplitude of the stray light, simply because it propagates in the same direction as the main beams. The value of a_s is taken to be equal to the value of the reflection coefficient of the AR coat, $a_s = 0.004$. This gives a value for $\Delta\phi$ of ± 0.4 nm. Table 5.9 summarises this uncertainty contribution.

Source	Size	k	Standard uncertainty	Sensitivity coefficient	Contribution
Uncertainty due to stray light	0.4	$\sqrt{3}$	0.23	1	0.23 nm
					0.23 nm

Table 5.9 Summation of uncertainties due to stray light

5.14 DEAD PATH LENGTH UNCERTAINTY

Dead path length, d, is defined as the difference in distance in air between the reference and measurement retroreflectors and the beamsplitter when the interferometer measurement is initiated (Zanoni 1988). Dead path error occurs when there is a non-zero dead path and environmental conditions change during a measurement. The equation below yields the displacement, D, for a single pass interferometer such as those used on NanoSurf IV

$$D = \frac{N\lambda_{vac}}{n_2} - \frac{\Delta n d}{n_2} \tag{5.39}$$

where N is half the number of fringes counted during the displacement, n_2 is the refractive index at the end of the measurement, Δn is the change in refractive index over the measurement time: that is $n_2 = n_1 + \Delta n$, and n_1 is the refractive index at the start of the measurement. The second term on the right hand side of equation (5.39) is the dead path error, L_{dp}.

Dead path error is corrected for in the software but there is still an uncertainty in the correction given by

$$u_c^2(L_{dp}) = \left(\frac{\partial L_{dp}}{\partial n_1}\right)^2 u_c^2(n_1) + \left(\frac{\partial L_{dp}}{\partial n_2}\right)^2 u_c^2(n_2) + \left(\frac{\partial L_{dp}}{\partial d}\right)^2 u_c^2(d) + \text{higher order terms} \quad (5.40)$$

The dead path imposes several critical measurement conditions on NanoSurf IV. Firstly, a sample must always be mounted such that the initial position is at the position of zero dead path. This can only be achieved to within 1 mm and $u_c^2(d)$ is ± 1 mm using a steel rule (plus the optical elements will be affected by thermal expansion and refractive index variations). Also, the environmental conditions have to be monitored. Any drifts in temperature of greater than ± 0.1 ^oC and pressure greater than ± 10 Pa void a measurement. Note that higher order terms in equation (5.40) are all negligible. Table 5.10 summarise the uncertainty in the measurement and correction for the dead path length.

Source	Size	k	Standard uncertainty	Sensitivity coefficient	Contribution
Uncertainty due dead path	0.20	$\sqrt{3}$	0.12	1	0.12 nm
					0.12 nm

Table 5.10 Summation of uncertainties due to dead path

5.15 UNCERTAINTIES DUE THE MEASUREMENT SET-UP

5.15.1 Cosine error

There will always be some misalignment of the measurement axis to the axis of motion of the stage. The measurement axis is the central line parallel to the in and out beams to and from the measurement retroreflector. The misalignment manifests itself as an error in the measured length that is directly proportional to the cosine of the angle between the measurement axis and the axis of motion of the stage. The cosine error always causes the interferometer to measure shorter than the actual distance travelled by the stage.

The cosine error in the x axis can be measured (and minimised) by removing the beamsplitter, attaching a mirror to the front of the measurement retroreflector and auto-reflecting the laser beam onto the output aperture of the laser. The alignment can then be checked as the stage is moved

through its full range. The worst case measured was a displacement from the aperture of less than 1 mm for a path length of around 1 m. This corresponds to a cosine error of 1.5 x 10^{-10} L and is negligible.

Provided the z interferometer block can be set up so as to get interference, the small length over which it operates ensures a negligible cosine error in this axis.

5.15.2 Abbe error

The causes and effects of the Abbe error are described elsewhere (Leach 2000). The Abbe offset has been made negligible in the z axis by virtue of the interferometer and probe design, *i.e.* the displacement measuring axis is co-axial with the displacement to be measured. In the x axis there can be an Abbe offset of up to 5 mm.

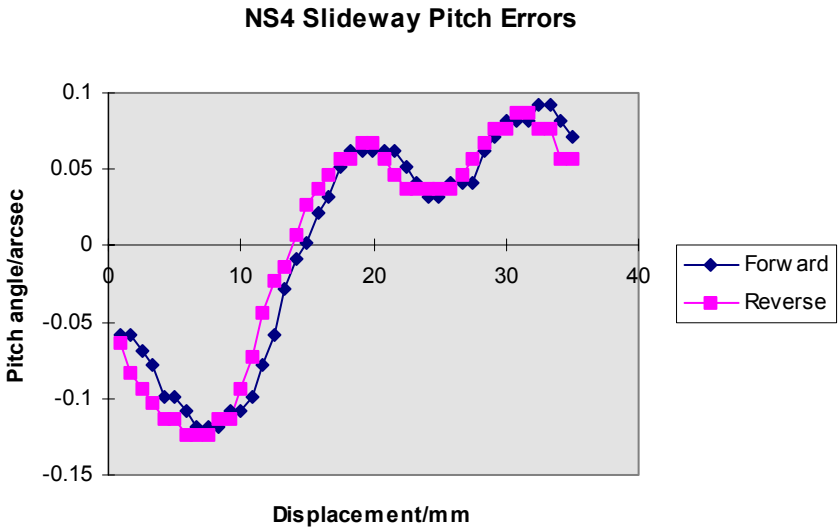

Figure 5.2 x axis slideway pitch errors

To determine the Abbe error in the x axis, the straightness of the slideway must be determined. This was carried out by setting up an autocollimator with a small aluminised microscope cover-slip epoxied to the front of the specimen mounting plate. To ensure that the slideway and autocollimator had the same mechanical earth (the stainless steel vibration isolation plate) a small, lightweight autocollimator was constructed from a compact disc reading head (Sony Model D50

Mk II, Armstrong & Fitzgerald 1992). The autocollimator has a resolution of 0.01 second of arc and was calibrated using an NPL indexing table (Moore 1440). Figures 5.2 and 5.3 show the straightness results for the *x* axis slideway. Note that there is no Abbe sensitivity to roll. From both the graphs it is apparent that the repeatability of these measurements is excellent when the direction of travel is reversed.

Over the full 35 mm travel range the pitch and yaw errors correspond to Abbe errors of 3.2 nm and 3.6 nm respectively. However, a typical measurement of surface texture would take place over less than 10 mm and over this displacement the Abbe error for both pitch and yaw is 0.84 nm. Table 5.11 shows the contribution of the Abbe error to the uncertainty.

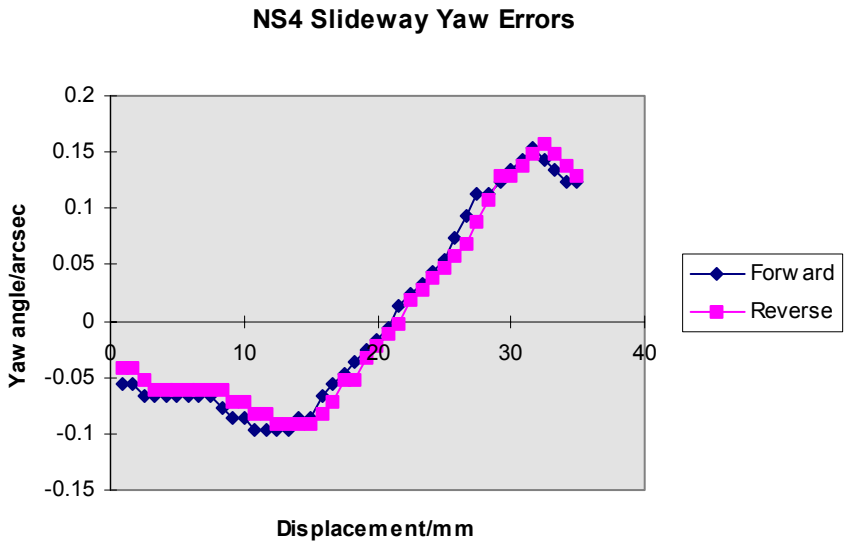

Figure 5.3 *x* axis slideway yaw errors

Source	Size	*k*	Standard uncertainty	Sensitivity coefficient	Contribution
Uncertainty due *x* straightness	0.02 arc sec	√3	0.49	1	0.49 nm
Resolution of autocollimator	0.01 arc sec	√12	0.07	1	0.07 nm
					0.59 nm

Table 5.11 Summation of uncertainties due to Abbe error

5.16 DEGREES OF FREEDOM OF THE INFLUENCE QUANTITIES

Table 5.12 lists the degrees of freedom associated with each source of measurement uncertainty plus the magnitude of the uncertainty.

Applying equation (5.4) gives an effective number of degrees of freedom of 45 .

5.17 EXPANDED UNCERTAINTY FOR A LENGTH MEASUREMENT

Adding the uncertainty contributions in table 5.12 in quadrature and multiplying by a coverage factor of k = 2 (justified with 45 degrees of freedom), gives the following combined standard uncertainty

$$u_c^{\,2}(L_x) = 2 \times \sqrt{0.66^2 + 1.5 \times 10^{-3} L^2} \tag{5.41}$$

Source of uncertainty	**Uncertainty / nm**	**Degrees of freedom**
Optical path difference	$\sqrt{(1 \times 10^{-2} L)^2 + 0.01}$	19
Air refractive index	$3.8 \times 10^{-2} L$	∞
Metrology frame & detection system	0.10	19
Imperfect optics & stray beams	0.23	∞
Deadpath length	0.12	∞
Abbe error	0.59	9

Table 5.12 Sources of uncertainty and their associated degrees of freedom. L is in millimetres.

As an example, if L_z were equal to 1 mm, then $u_c^2(L_z)$ = 1.322 nm and if L_z = 1 nm, $u_c^2(L_z)$ = 1.320 nm. It is clear that in most cases the length dependent uncertainty contribution is negligible. The uncertainty in NanoSurf IV is quoted as 1.320 nm at k = 2 with 45 degrees of freedom.

5.18 UNCERTAINTIES IN MEASURING SURFACE TEXTURE PARAMETERS

In order to put a meaningful number to measured surface texture data and aid in understanding the functionality of a surface, various parameters, such as the average or peak-to-valley height, can be calculated. It is extremely rare to see rigorous uncertainty analysis applied to the calculation of uncertainty in a parameter. This section applies the guidelines laid down in the *GUM* to calculate the uncertainty in a given surface texture parameter. Only the parameters advocated by the ISO standards are considered. Note that the effects of any mechanical, electrical or computational filtering of the measured data are not considered here (with the exception of the calculation of the average reference line).

5.19 REFERENCE DATA

To obtain a reference data set, a 0.2 mm trace of an optical flat (NPL specimen D19) was taken at a speed of 0.1 mm per minute. The x and z displacements were measured at 2048 sampling points. A first-order polynomial least-squares fit was removed from the data - this filtering is necessary due to the lack of levelling of the specimen. The dominant frequency component that is clearly evident in the trace is the resonant frequency of the probing system. As this is only a reference set of data, no post measurement filtering or de-trending has been carried out (Rothe, Duparré, *et. al.* 1994). All calculations were carried out using MATLAB (MathWorks Inc.) to ensure the reliability of any mathematical algorithms. Figure 5.4 presents the first 150 data points.

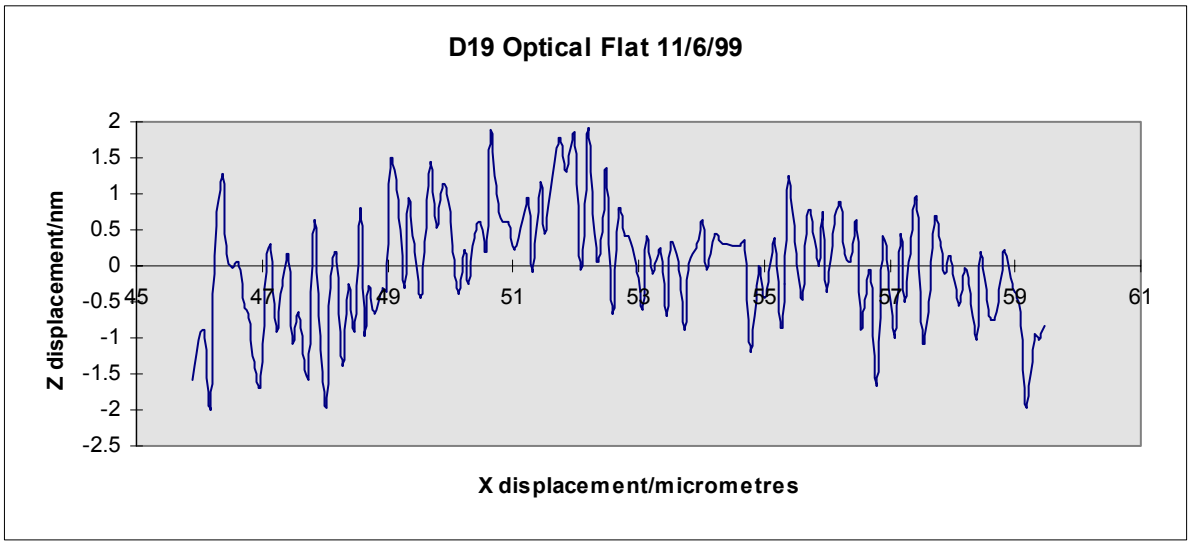

Figure 5.4 The reference data

5.20 UNCERTAINTY IN THE CALCULATION OF THE AVERAGE REFERENCE LINE

Before most parameters can be calculated a average reference line has to be fitted to the x and z data. The fitting equation is given by

$$z = a + bx \tag{5.43}$$

where a is the intercept on the z axis and b is the gradient. Uncertainties in a an b must be propagated through to the parameters.

To find $u(a)$ and $u(b)$ we must carry out a least-squares fit to the measured data assuming there are errors in both x and z. In the general case, this problem has no analytical solution, but when $u(x)$ can be assumed proportional to $u(z)$, as is the case with NanoSurf IV, the problem can be circumvented (Bruzzone & Moreno 1998). When only uncertainties in z are considered, the least-squares fitting requires the minimisation of

$$\chi^2 = \sum_{i=1}^{n} \frac{\left(z_i - a - bx_i\right)^2}{u^2(z_i)}. \tag{5.44}$$

The problem has the solutions

$$b^* = \frac{SS_{xz} - S_x S_z}{SS_{xx} - S_x^2} \text{ and } a^* = \frac{S_{xx} S_z - S_x S_{xz}}{SS_{xx} - S_x^2} \tag{5.45}$$

where

$$S = \sum_{i=1}^{n} \frac{1}{u^2(z_i)} \qquad S_x = \sum_{i=1}^{n} \frac{x_i}{u^2(z_i)} \qquad S_z = \sum_{i=1}^{n} \frac{z_i}{u^2(z_i)}$$

$$S_{xx} = \sum_{i=1}^{n} \frac{x_i^2}{u^2(z_i)} \qquad S_{zz} = \sum_{i=1}^{n} \frac{z_i^2}{u^2(z_i)} \qquad S_{xz} = \sum_{i=1}^{n} \frac{x_i z_i}{u^2(z_i)} \tag{5.46}$$

The fit parameters' uncertainties are then given by

$$u(a^*) = \sqrt{\frac{S_{xx}}{SS_{xx} - S_x^2}} \text{ and } u(b^*) = \sqrt{\frac{S}{SS_{xx} - S_x^2}}. \tag{5.47}$$

If errors in both co-ordinates are considered, the effective variance method states that the expression (Barker & Diana 1974)

$$\chi^2 = \sum_{i=1}^{n} \frac{\left(z_i - a - bx_i\right)^2}{u^2(z_i) + u^2(x_i)} \tag{5.48}$$

must be minimised. Equation (5.48) has no analytical solution in the general case. However, provided $u(x) = du(z)$, where d is a constant (unity in the case of NanoSurf IV), equation (5.48) reduces to

$$\chi^2 = \frac{1}{1 + b^2 d^2} \sum_{i=1}^{n} \frac{(z_i - a - bx_i)}{u^2(z_i)}. \tag{5.49}$$

Minimisation of equation (5.49) leads to a quadratic expression for b, but only the root given here is to be considered (Bruzzone & Moreno 1999)

$$db = \frac{1}{2}\left\{ -\frac{1}{db^*} + \frac{db^*}{r^2} + \frac{1}{db^*}\left[\left(1 - \frac{(db^*)^2}{r^2}\right)^2 + 4(db^*)^2 \right]^{1/2} \right\} \tag{5.50}$$

where r is the linear correlation coefficient, given by

$$r^2 = \frac{\left(SS_{xz} - S_x S_z\right)^2}{\left(SS_{xx} - S_x^2\right)\left(SS_{zz} - S_z^2\right)}. \tag{5.51}$$

Once the slope b has been obtained, it is possible to evaluate a by means of

$$a = \frac{S_z - S_x b}{S}. \tag{5.52}$$

For the case of proportional errors in x and z, the uncertainties in a and b can be found from the following

$$u^2(b) = u^2(b^*) f(db^*, r^2) \tag{5.53}$$

and

$$u^2(a) = \frac{1+b^2d^2}{S}\left\{1+[u^2(a^*)S-1]f(db^*,r^2)\right\} \tag{5.54}$$

where

$$f(db^*,r^2) = (1+b^2d^2)^2\,\frac{1+(db^*)^2/r^2}{\left[1+d^2(2bb^*-b^{*2}/r^2)\right]^2}\,. \tag{5.55}$$

For the reference data set the uncertainties are $u(a)$ = 0.46 nm and $u(b)$ = 8.7 x 10^{-6}. Assuming these uncertainties are rectangularly distributed, they must be divided by $\sqrt{3}$. Once the calculated least-squares curve has been removed from the data, a given value of z_i is given by

$$z_i' = z_i - (a+bx_i)\,. \tag{5.56}$$

An uncertainty in z' is now given by the following equation

$$u^2(z') = u^2(z) + u^2(a) + x^2u^2(b) + b^2u^2(x)\,. \tag{5.57}$$

5.21 UNCERTAINTIES IN THE PARAMETERS

A list and short description of the surface texture parameters in ISO 4287: 1997 (*Geometrical product specifications (GPS) - Surface texture: Profile method - Terms, definitions and surface texture parameters*) is given in table 5.13. Where a parameter only applies to one length measurement, for example *Rp*, equation 5.41 should be applied appropriately. Where a parameter is the sum of parameters calculated for their corresponding sampling lengths over the entire evaluation length, a simple quadrature sum should be applied.

Name & symbol	**Short description**
profile peak height, *Zp*	distance between the *x* axis and the highest point of the profile peak

profile valley height, *Zv*	distance between the *x* axis and the lowest point of the profile valley
profile element height, *Zt*	sum of the height of the peak and depth of the valley of a profile element
profile element width, *Xs*	length of the *x* axis segment intersecting with the profile element
material length of profile at level *c*, *M(c)*	sum of the section lengths obtained, intersecting with the profile element by a line parallel to the *x* axis at a given level *c*
maximum profile peak height, *Rp*	largest profile peak height within a sampling length
maximum profile valley depth, *Rv*	largest profile valley depth within a sampling length
maximum height of profile, *Rz*	sum of height of the largest profile peak height and the largest profile valley within a sampling length
mean height of profile elements, *Rc*	mean value of the profile element heights *Zt* within a sampling length $$Rc = \frac{1}{m}\sum_{i=1}^{m} Zt_i$$
total height of profile, *Rt*	sum of the height of the largest profile peak height *Zp* and the largest profile valley depth *Zv* within the evaluation length
arithmetical mean deviation of the assessed profile, *Ra*	arithmetic mean of the absolute ordinate values *Z(x)* within a sampling length $$Ra = \frac{1}{l}\int_0^l \left|Z(x)\right| dx$$
root mean square deviation of the assessed profile, *Rq*	root mean square value of the ordinate values *Z(x)* with the sampling length $$Rq = \sqrt{\frac{1}{l}\int_0^l Z^2(x)dx}$$
skewness of the assessed profile, *Rsk*	quotient of the mean cube value of the ordinate values *Z(x)* and the cube of *Rq* respectively within the sampling length $$Rsk = \frac{1}{Rq^3}\left[\frac{1}{l}\int_0^l Z^3(x)dx\right]$$
kurtosis of the assessed profile, *Rku*	quotient of the mean quartic value of the ordinate values *Z(x)* and the fourth power of *Rq* respectively within the sampling length

	$$Rku = \frac{1}{Rq^4}\left[\frac{1}{l}\int_0^l Z^4(x)dx\right]$$
mean width of the profile elements, *RSm*	mean value of the profile element widths *Xs* within a sampling length $$RSm = \frac{1}{m}\sum_{i=1}^{m} Xs_i$$
root mean square slope of the assesses profile, *RΔq*	root mean square value of the ordinate slopes *dZ/dX*, within the sampling length
material ratio of the profile, *Rmr(c)*	ratio of the material length of the profile elements *Ml(c)* at a given level *c* to the evaluation length $$Rmr(c) = \frac{Ml(c)}{l}$$
profile section height difference, *Rδc*	vertical distance between two section levels of given material ratio $$R\delta c = C(Rmr1) - C(Rmr2);\ (Rmr1 < Rmr2)$$
relative material ratio, *Rmr*	material ratio determined at a profile section *Rδc*, related to reference *C*0 $$Rmr = Rmr(C1)$$ where $$C1 = C0 - R\delta c$$ $$C0 = C(Rmr0)$$

Table 5.14 Surface texture parameters

5.21.1 Uncertainty in *Ra*

The equation given in table 5.14 for *Ra* is for continuous data sampling within the sampling length. For the case of a real surface texture measuring instrument, with a finite sampling length, *Ra* is given by

$$Ra = \frac{1}{N}\sum_{i=1}^{N}\left|Z_i\right|. \qquad (5.58)$$

To calculate the uncertainty, $u_c(Ra)$, equation (5.1) is applied to equation (5.58), *i.e.*

$$u_c^2(Ra) = c_{z_i}^2 u^2(z_i) = \frac{1}{N}\sum_{i=1}^{N} u^2(z_i) \tag{5.59}$$

where all the higher order terms are equal to zero. The combined standard uncertainty of the *Ra* parameter is simply the sum of the individual uncertainties divided by the number of samples, or the average uncertainty. There is, however, a subtlety here. By definition, it is not physically possible to have a negative *Ra*. But, if it is assumed that the measurement uncertainties are normally distributed, it is possible to have a confidence interval that allows negative *Ra* values. For example, *Ra* = 0.1 nm ± 0.5 nm could have values of *Ra* that vary from -0.4 nm to 0.6 nm. The problem has arisen due to the arbitrary assumption that the uncertainties in *Ra* are normally distributed about the "true value", whereas the mathematical definition of *Ra* rules this assumption out - any measurement noise will positively bias the value of *Ra*. As each surface will have a different distribution of surface heights, a value for *Ra* can only be stated with a standard uncertainty - to state an expanded uncertainty has implied that we have prior knowledge of the height distribution of the surface. Of course, the distribution could be calculated for each surface, but this would not be practical without rigorous software backup.

For the reference data set, *Ra* = 0.65 nm and its standard uncertainty is 0.5 nm.

5.21.2 Uncertainty in *Rq*

The equation for a sampled evaluation of *Rq* is given by

$$Rq = \sqrt{\frac{1}{N}\sum_{i=1}^{N} Z_i^2} \tag{5.60}$$

The associated uncertainty in *Rq* is given by

$$u_c^2(Rq) = c_{z_i}^2 u^2(z_i) = \frac{1}{N}\frac{1}{Rq}\sum_{i=1}^{N} {z_i}^2 u^2(z_i)\,. \tag{5.61}$$

The higher order terms are not equal to zero but will be negligibly small. For the reference data set *Rq* = 1.4 nm with a standard uncertainty of 0.30 nm. Again, because the value for *Rq* is always positive, the same points raised above for *Ra* apply for *Rq*.

5.21.3 Uncertainty in *Rsk* and *Rku*

The uncertainties in the skewness and kurtosis of a surface cannot be calculated using the guidelines laid down in the *GUM.* This is because they are defined parameters calculated from the data. There definitions lead to complexities with the higher order terms that give nonsensible results.

6. DISCUSSION

In §2 a number of methods, both historical and current, were described for calibrating a surface texture measuring instrument. No other area of dimensional metrology has such a vast armoury of methodologies and parameters available to choose from when applying metrology. This situation must be rationalised. Most instruments are calibrated using some form of specimen with a 'known' surface texture (or at least a 'known' value for a surface texture parameter). These specimens have not always been calibrated in both lateral and vertical directions.

NanoSurf IV is a surface texture measuring instrument that measures the co-ordinates of points on a surface in two-dimensions (assuming it is operating in its measurement bandwidth). The instrument is designed primarily to calibrate surface texture standard specimens that can be in-turn used to calibrate other instruments. The author sees this as the way forward.

Uncertainty analysis is a complicated and time-consuming process that must be applied, at the very least, to instruments in the calibration chain such as NanoSurf IV. This would make it easier for an instrument lower down the chain of accuracy to simply apply calibrated specimens as a simple check for instrument performance. NPL is currently developing a series of sinusoidal (in the first instance) samples to bridge the gap between instruments like NanoSurf IV and those in industry.

7. ACKNOWLEDGEMENTS

The authors would like to thank Keith Jackson (NPL) and Dr Derek Chetwynd (Warwick University) for help with the technical aspects of this report. The work was funded by the DTI as part of the NMS Programme for Length 1997-1999.

8. REFERENCES

Armstrong T R, Fitzgerald M P 1992 An autocollimator based on the laser head of a compact disc player *Meas. Sci. Technol.* **3** 1072-1076

Barker D R, Diana L M 1974 Simple method for fitting data when both variables have uncertainties *Am. J. Phys.* **42** 223-227

Bendeli A, Duruz J, Thwaite E G 1974 A surface simulator for precise calibration of surface roughness measuring equipment *Metrologia* **10** 137-143

Bönsch G, Potulski E 1998 Measurement of the refractive index of air and comparison with the Edlén formulae *Metrologia* **35** 133-139

Bruzzone H, Moreno C 1998 When errors in both coordinates make a difference in the fitting of straight lines by least squares *Meas. Sci. Technol.* **9** 2007-2011

Chetwynd D G, Siddons D P, Bowen D K 1983 X-ray interferometer calibration of microdisplacement transducers *J. Phys. E: Sci. Instrum.* **16** 871-874

Decker J E, Ulrich A, Pekelsky J R 1998 Uncertainty of gauge block calibration by mechanical comparison: a worked example for gauge blocks of dissimilar materials *Proc. SPIE* **3477** 225-246

Downs M J, Ferris D H, Ward R E 1990 Improving the accuracy of the temperature measurement for gases by correction for the response delays in the thermal sensors *Meas. Sci. Technol.* **1** 717-719

Downs M J 1998 Realisation of the optimum performance from length-measuring interferometers by atmospheric refractometry *Proc. SPIE* **3477** 46-53

Franks A 1993 Progress towards traceable nanometric surface metrology *Nanotechnology* **4** 200-205

Griffith J E 1993 Dimensional metrology with scanning probe microscopes *J. Appl. Phys.* **74** R83-R109

Haitjema H 1997 International comparison of depth-setting standards *Metrologia* **34** 161-167

Haitjema H 1998 Uncertainty analysis of roughness standard calibration using stylus instruments *Prec. Eng.* **22** 110-119

Hariharan P 1997 Interferometric measurements of small-scale surface irregularities: sources of errors *Opt. Eng.* **36** 2330-2334

Hume K J 1980 *A history of engineering metrology* (Mechanical Engineering Publications Ltd) ch. 8

Jφrgensen J F, Garnaes J, Thulstrup D, Rasmussen S E 1997 Calibrated surface characterization, problems and solutions *7th Int. Conf. on Metrology and Properties of Engineering surfaces* 358-365

Leach R K 2000 *NanoSurf IV: Traceable surface texture measurement at the nanometre level* (PhD Thesis: Warwick University) to be published

Mana G 1989 Diffraction effects in optical interferometers illuminated by laser sources *Metrologia* **26** 87-93

National Measurement System Programme for Length 1996-1999 MPU 7/28.18

Petru F, Cíp O 1999 Problems regarding linearity of data of a laser interferometer with a single-frequency laser *Prec. Eng.* **23** 39-50

Reason R E 1967 *ASTME Intern. Conf. On Manufacturing Technology,* Ann Arbor, Michigen

Rothe H, Duparré A, Jacobs S 1994 Generic detrending of surface profiles *Opt. Eng.* **33** 3023-3030

Schobinger J P 1959 *Investigation into the production of roughness standards* (PhD thesis: Federal Technical College, Zürich)

Self S A 1983 Focussing of spherical Gaussian beams *Appl. Opt.* **22** 658-661

Sharman H B 1967 Calibration of surface texture measuring instruments *Proc. Instn. Mech. Engnrs.* **182** 319-326

Sheer B W, Stover J C 1998 Development of a smooth-surface microroughness standard *Proc SPIE* **3141** 78-87

Song 1988 Random profile precision roughness calibration specimens *Surface Topography* **1** 303-314

Standards Infobase 1998 (ILI: Berkshire)

Stedman M 1987 Basis for comparing the performance of surface-measuring machines *Prec. Eng.* **9** 149-152

Teague E C 1978 Uncertainties in calibrating a stylus type surface texture measuring instrument with an interferometrically measured step *Metrologia* **14** 39-44

Timms C 1946 Measurement of surface roughness *Metal Treatment* **13** 111

Tsukada T, Kanada T 1986 Evaluation of two- and three-dimensional surface roughness profiles and their confidence *Wear* **109** 69-78

Underwood A 1953 Two recent developments for accurate measurement of surface texture *Proc. Symp. on Engineering Dimensional Metrology, NPL* **II** 621

Van Hasselt R, De Bruin W 1963 Comparative investigation of industrial surface-roughness measuring instruments *Ann. CIRP* **XI** 193

Watts R A, Samble J R, Hutley M C, Preiest T W, Lawrence C R 1997 A new optical technique for characterizating reference artefacts for surface profilometry *Nanotechnology* **8** 35-39

Whitehouse D J 1988 Nano-calibration of stylus-based surface measurements *J. Phys. E: Sci. Instrum.* **21** 46-51

Whitehouse D J 1994 *Handbook of surface metrology* (Institute of Physics Publishing)

Yule G U, Kendall M G 1937 *An introduction to the theory of statistics* (Charles Griffin: London)

Zanoni C A 1988 *High precision interferometric linear and angular displacement interferometry* Zygo Corporation document